JACS
JOURNAL OF THE AMERICAN CHEMICAL SOCIETY
Article
pubs.acs.org/JACS

Metallic Nickel Nitride Nanosheets Realizing Enhanced Electrochemical Water Oxidation

Kun Xu,[⊥,†] Pengzuo Chen,[⊥,†] Xiuling Li,[‡] Yun Tong,[†] Hui Ding,[†] Xiaojun Wu,[†,‡] Wangsheng Chu,*[,§] Zhenmeng Peng,*[,∥] Changzheng Wu,*[,†] and Yi Xie[†]

[†]Hefei National Laboratory for Physical Sciences at the Microscale, Collaborative Innovation Center of Chemistry for Energy Materials, University of Science and Technology of China, Hefei, Anhui 230026, PR China

[‡]CAS Key Laboratory of Materials for Energy Conversion and Department of Material Science and Engineering, University of Science and Technology of China, Hefei, Anhui 230026, PR China

[§]National Synchrotron Radiation Laboratory, University of Science and Technology of China, Hefei, Anhui 230029, PR China

[∥]Department of Chemical and Biomolecular Engineering, University of Akron, Akron, Ohio 44325, United States

Supporting Information

ABSTRACT: Exploring efficient and inexpensive oxygen evolution reaction (OER) electrocatalysts is of great importance for various electrochemical energy storage and conversion technologies. Ni-based electrocatalysts have been actively pursued because of their promising activity and earth abundance. However, the OER efficiency for most of the developed Ni-based electrocatalysts has been intrinsically limited due to their low electrical conductivity and poor active site exposure yield. Herein, we report metallic Ni_3N nanosheets as an efficient OER electrocatalyst for the first time. The first-principles calculations and electrical transport property measurements unravel that the Ni_3N is intrinsically metallic, and the carrier concentration can be remarkably improved with dimensional confinement. The EXAFS spectra provide solid evidence that the Ni_3N nanosheets have disordered structure resultant of dimensional reduction, which then could provide more active sites for OER. Benefiting from enhanced electrical conductivity with metallic behavior and atomically disordered structure, the Ni_3N nanosheets realize intrinsically improved OER activity compared with bulk Ni_3N and NiO nanosheets. Our finding suggests that metallic nitride nanosheets could serve as a new group of OER electrocatalysts with excellent property.

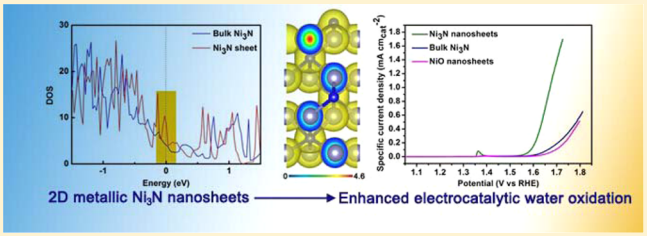

INTRODUCTION

The oxygen evolution reaction (OER) has attracted great research attention in recent years because of its vital role in various energy conversion and storage technologies, such as water splitting for hydrogen production, regenerative fuel cells and metal-air batteries, and so on.[1−3] The OER has intrinsically very sluggish reaction kinetics, caused by the involved multi proton-couple electron transfer steps, and requires the use of electrocatalyst for promoting the reaction rate.[4,5] Up to date, IrO_2 and RuO_2 still represent the most efficient electrocatalysts for the reaction.[6,7] The scarcity and thus high cost of the noble metals, however, have greatly hampered their practical application on a large scale. Therefore, it is highly desirable and imperative to develop new OER electrocatlysts with both excellent property and low cost.

Thanks to earth abundant nature, environmental benignity, and unique 3d electron number and special e_g orbitals, nickel-based compounds have been discovered as good OER catalyst candidates. Great efforts have been devoted to study of the OER property of Ni-based structures, spanning from nickel oxides,[8−10] nickel-hydroxide,[11] nickel-oxyhydroxide,[12] Ni-based layer double hydroxide[13−16] to nickel sulfides.[17] However, one big deficiency of these Ni-based electrocatalysts is their poor electron conductivity. These materials are either semiconducting or insulating, which greatly impede the electron transportation from catalyst surface to the support electrode.[18] Moreover, the poor electron conductivity causes formation of Schottky barriers at both catalyst−electrolyte and catalyst−support electrode interfaces. Additional overpotential is needed to overcome these energy barriers, leading to decreased energy conversion efficiency.[19] Owing to these facts, it is apparent that the OER efficiency of current Ni-based electrocatalysts has been greatly limited by their intrinsic inferior electrical conductivity. From this viewpoint, new Ni-based structure with high electron conductivity would be more efficient OER catalyst than the semiconducting/insulating counterparts and is thus of high desire.

Theoretical investigation inspires the research of 2D Ni_3N nanosheets as a novel Ni-based OER electrocatalyst. As shown in Figure 1a, the calculated density of states (DOS) of bulk

Received: November 21, 2014
Published: March 11, 2015

DOI: 10.1021/ja5119495
J. Am. Chem. Soc. 2015, 137, 4119−4125

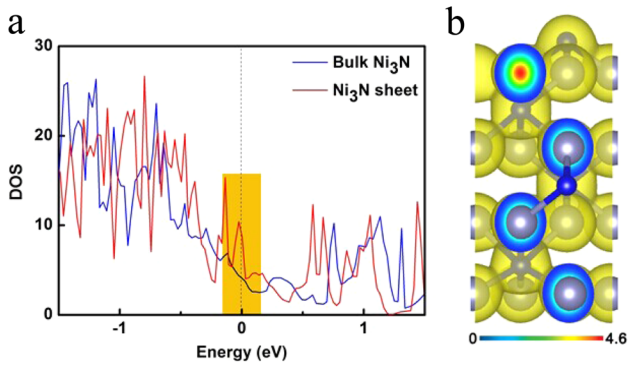

Figure 1. (a) Calculated density of states for bulk Ni_3N and Ni_3N sheet. The Fermi level is set at 0 eV. (b) Charge density waves for the Ni_3N sheet, plotted from 0 (blue) to 4.6 eÅ^{-3} (red).

Ni_3N are continuous near the Fermi level, indicating that Ni_3N is intrinsically metallic. Interestingly, the DOS of Ni_3N sheet (Figure 1a) near the Fermi level is more intense than that of bulk Ni_3N. It suggests that the electrical property of Ni_3N, in particular the carrier concentration and the electrical conductivity, can be further improved when a dimensional confinement is imposed. Meanwhile, the OER property could benefit from planar configuration of 2D Ni_3N nanosheets, which offer large specific surface area and intimate contact with support electrodes.[20,21] Also, the structure of atomically thick nanosheets are often disordered, which could provide more active sites for OER.[18,21,22] In this regard, 2D metallic Ni_3N nanosheets could potentially be an excellent OER electrocatalyst.

Despite the great promise as OER catalyst, there is little research on 2D metallic Ni_3N nanosheets up to date, primarily due to a lack of effective methods for the synthesis of nonlayer nickel nitride nanosheets. Herein, for the first time, we report successful synthesis of 2D Ni_3N nanosheets with an average sheet thickness of less than 3 nm, as a new metallic graphene-like material. The prepared Ni_3N nanosheets show good electrical conductivity with disordered structure. They exhibit much higher OER activity than both bulk Ni_3N and NiO nanosheets, and have excellent stability. Our work would open a new door for the design of highly efficient OER electrocatalysts based on metallic state materials.

EXPERIMENTAL SECTION

Synthesis of Ni-Based Nanosheet Precursor. The Ni-based nanosheets precursor was prepared using a modified method which was reported by previous literature.[23] In a typical experiment, 2 mmol nickel acetate and 4 mmol hexamethylenetetramine (HMT) were dissolved in 35 mL of distilled water under vigorous stirring for 30 min to form a transparent solution. Then the mixture was transferred into a 40 mL Teflon-lined autoclave, sealed and heated at 120 °C for 12 h. The system was allowed to cool down to room temperature, and the final product was collected by centrifuging the mixture, washed with water and ethanol for several times and then dried in a vacuum overnight for further characterizations.

Synthesis of NiO Nanosheets. The NiO nanosheets were obtained from Ni-based nanosheets precursor by a simple calcination reaction. In a typical procedure, 500 mg of Ni-based precursor was placed in the tube furnace. The furnace was heated to 500 °C with a rate of 10 °C min^{-1} in air and maintained for 3 h. Then the final products were collected for further characterization.

Synthesis of Ni_3N Nanosheets. In a typical experiment, 100 mg Ni-based nanosheets precursor was placed in the tube and heated to 380 °C with a rate of 10 °C min^{-1} under a flowing NH_3 atmosphere (1 bar, 500 sccm). After reacting 3 h at 380 °C, the system was allowed to cool down to room temperature naturally still under a flowing NH_3 atmosphere (1 bar, 500 sccm). Finally, the black products were collected for further characterization

Synthesis of Bulk Ni_3N. The bulk Ni_3N was obtained according to previous literature.[24] In a typical process, 1.5 g of $Ni(NO_3)_2{\cdot}6H_2O$ powders were added into 10 mL of ammonia solution slowly under rapid stirring to obtain a blue crystalline complex. Then the $[Ni(NH_3)_6](NO_3)_2$ complex was placed in the tube furnace and heated at 380 °C under a flowing NH_3 atmosphere (1 bar, 500 sccm) to prepare black bulk Ni_3N sample.

Preparation of Ni Precursor/CC. In a typical synthesis, carbon cloths (CC) were activated by cleaning carefully with concentrated HNO_3, and then washed in succession with deionized water, acetone, and ethanol for several times. Next, 5 mmol $Ni(NO_3)_2{\cdot}6H_2O$ and 10 mmol HMT was dissolved in 35 mL of deionized water under vigorous stirring for 15 min, and then a cleaned CC (1 cm × 1.5 cm) was immersed into above solution for another 20 min. The solution and CC were transferred to a 40 mL Teflon-lined stainless-steel autoclave and maintained at 120 °C for 12 h. After the autoclave was allowed to cool down to room temperature, the Ni precursor/CC was washed with water, ethanol for several times and dried in a vacuum.

Preparation of Ni_3N Nanosheets/CC. In a typical procedure, a piece of Ni precursor/CC was placed in a tube furnace. Next, the furnace was heated to 380 °C at 10 °C min^{-1} under a flowing NH_3 atmosphere (1 bar, 500 sccm) and maintained for 3 h, and then allowed to cool to room temperature.

Materials Characterization. X-ray powder diffraction (XRD) was performed by using a Philips X'Pert Pro Super diffractometer with Cu Kα radiation (λ = 1.54178 Å). X-ray photoelectron spectra (XPS) were obtained on an ESCALAB MK II X-ray photoelectron spectrometer with Mg Kα as the excitation source. Atomic force microscopy (AFM) images were carried out on a DI Innova scanning probe microscope. The transmission electron microscopy (TEM) and high-resolution TEM (HR-TEM) were performed on a JEM-2100F field emission electron microscope at an acceleration voltage of 200 kV. The field emission scanning electron microscopy (FE-SEM) images were taken on a JEOL JSM-6700F SEM. The high-angle annular dark-field scanning transmission electron microscopy (HAADF-STEM) image and EDS mapping images were taken on a JEOL JEM-ARF200F atomic resolution analytical microscope. The electrical transport property measurement were carried out using a Keithley 4200-SCS semiconductor Characterization system and a four-point probe method. The Ni K-edge absorption spectra were measured at the 1W1B beamline of the Beijing Synchrotron Radiation Facility (BSRF). The storage ring was operated at 2.5 GeV, with the electron current decreasing from 240 to 160 mA within about 8 h. The nitrogen adsorption−desorption isotherms were measured using a Micromeritics ASAP 2000 system at 77K.

Calculation Method. First-principle calculations were carried out using density-functional theory (DFT)[25,26] implemented in the VASP package.[27,28] The generalized-gradient approximation (GGA) in the Perdew−Burke−Ernzerhof (PBE) form[29] and the projector augmented wave (PAW) approach[30] are employed. The cutoff energy for plane wave is 500 eV. During geometric optimization, the Brillouin zone are sampled with 5 × 5 × 5 and 7 × 7 × 1 mesh for bulk Ni_3N and Ni_3N single layers, respectively. A denser k-points grid of 7 × 7 × 7 and 15 × 15 × 1 are used for calculating the densities of states (DOS).The thickness of vacuum space is set to be 15 Å.

Electrochemical Measurements. All the electrochemical measurements were performed in a three-electrode system on an electrochemical workstation (CHI660B). In a typical procedure, 4 mg of catalysts and 35 μL of 5 wt % Nafion solutions (Sigma-Aldrich) were dispersed in 1 mL of water−isopropanol solution with volume ratio of 3:1 with sonication for 30 min to form a homogeneous ink. The 5 μL of the above dispersion was load onto a glassy carbon electrode of 3 mm in diameter (loading 0.285

DOI: 10.1021/ja5119495
J. Am. Chem. Soc. 2015, 137, 4119−4125

mg cm^{-2}). Linear sweep voltammetry with a scan rate of 5 mV s^{-1} was conducted in 1 M KOH solution (purged with oxygen for 30 min) using Ag/AgCl (3.3 mol/L KCl) electrode as the reference electrode, the platinum gauze as the counter electrode, and the glassy carbon electrode with various catalysts as the working electrode. Electrochemical impedance spectroscopy (EIS) measurements of the various catalysts were carried out using above three electrode systems at 0.607 V vs Ag/AgCl. The frequency range was 100 K Hz to 0.1 Hz, and the amplitude of the applied voltage was 5 mV.

RESULTS AND DISCUSSION

Precursor morphology-directed strategy has been proven to be effective for preparation of nitride compounds with specific morphology.[31] In our case, Ni-based precursor nanosheets were first synthesized and then used to prepare Ni_3N nanosheets. Nickel nitride nanosheets were prepared by direct calcination of the Ni-based precursor nanosheets at 380 °C under an NH_3 atmosphere, while the NiO ultrathin nanosheets were obtained by direct calcination of the Ni-based precursor nanosheets at 500 °C in air. The overall reaction can be described using the following equation:

$$6Ni(OH)_2 + 4NH_3 = 2Ni_3N + 12H_2O + N_2$$

Structural information on the nitrided sample was investigated by X-ray diffraction (XRD). As shown in Figure 2a, all the diffraction peaks could be well indexed to

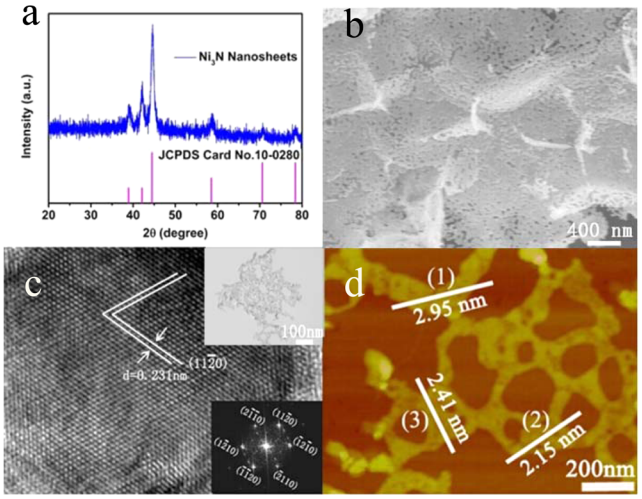

Figure 2. Characterization of Ni_3N nanosheets. (a) XRD pattern. (b) SEM image. (c) HRTEM image. Inset: corresponding FFT pattern and TEM image. (d) AFM image.

hexagonal Ni_3N (JCPDS Card No.10−0280; Space group: $P6322$; $a = b = 4.621$ Å; $c = 4.304$ Å), with no detectable impurities. In order to obtain the morphology and microstructural information on the as-synthesized Ni_3N nanosheets, detailed microscopic characterizations were performed. As shown in Figure 2b, the scanning electron microscopy (SEM) image demonstrates clearly the as-prepared Ni_3N samples consist of uniform 2D nanosheets with unique porosity. Meanwhile, the transmission electron microscopy (TEM) image presented in Figure 2c also confirms that our as-prepared samples are porous nanosheets. The average pore diameter is approximately 50 nm, which has been illustrated by BJH adsorption $dV/d(\log(D))$ pore volume (Figure S6, Supporting Information). The HRTEM image and corresponding fast Fourier transform (FFT) pattern clearly reveal that the nanosheet is a hexagonal single crystal with c-axis crystalline orientation (Figure 2c). Atomic force microscopy (AFM) was used to evaluate thickness of as-synthesized nanosheets. As can be seen from Figure 2d, the average scanning heights of the Ni_3N nanosheets are ranging from 2.15 to 2.95 nm, which indicates that the nanosheets consist of about 5−7 unit cells (a single Ni_3N unit cell along the c direction is 0.43 nm). All results clearly confirm that porous Ni_3N nanosheets have been successfully prepared.

Microscopic elemental compositions of Ni_3N nanosheets were further investigated using energy dispersive X-ray (EDX). As presented in Figure S7a, the EDX measurements found that Ni and N were the only elements composing of the Ni_3N nanosheets (Cu and C derived from Cu grid). The elemental distribution throughout the nanosheets was further examined using HAADF-STEM and corresponding elemental mappings, as shown in Figure S7b−d. It was noted that different colors were used to distinguish the distributions of Ni (indicated by blue color) and N (indicated by red color) elements, with areas in a brighter color representing more concentrated element in these regions. Both the Ni and N elements were found with homogeneous distribution within the Ni_3N ultrathin nanosheets. In a word, the prepared Ni_3N nanosheets were uniform in composition and had no detectable impurities. The high quality Ni_3N ultrathin nanosheets provided an ideal platform and prerequisite for further study of their intrinsic physicochemical properties.

In order to verify whether Ni_3N nanosheets are metallic with enhanced electrical conductivity compared with bulk counterpart, the temperature-dependent resistivity measurements were carried out. The electrical behaviors of as prepared Ni_3N nanosheets and bulk Ni_3N are given in Figure 3a (note: NiO is insulator). As expected, temperature dependence of resistivity of the Ni_3N nanosheets clearly takes on a slightly increasing electrical resistivity with the increasing temperature, indicating an intrinsic metallic state of Ni_3N nanosheets. Although electrical behavior of bulk Ni_3N is similar to that of Ni_3N nanosheets, the value of resistivity of Ni_3N nanosheets (10.9×10^{-5} Ω·m at 300 K) is approximately 3.8 times lower than that of the bulk counterpart. These experimental results on electrical behavior are consistent with that from the first-principle calculations. Therefore, the intrinsic metallic state and enhanced electrical conductivity in 2D Ni_3N nanosheets would ensure fast electron transport between catalyst-electrolyte and catalyst−support electrode interfaces, showing a promising sign for further promoting electrochemical performance as electrocatalyts for water oxidation.

Extended X-ray absorption fine structure spectroscopy (EXAFS) measurements at the Ni K-edge were also carried out to investigate the local geometrical structure of Ni_3N nanosheets, using the bulk Ni_3N for reference sample. In Figure 3b, the Ni K-edge EXAFS of Ni_3N nanosheets presented a similar oscillation with a remarkable amplitude reduction, indicating the different local atomic arrangements of the nanosheets (Table S1). This amplitude reduction could be further illustrated by the corresponding Fourier transforms (FTs), as shown in Figure 3c. FTs present two peaks in the range of 1−3 Å. The first is corresponding to Ni−N correlation and the second is Ni−Ni pair. Intensities of the Ni−N pairs of the two samples are almost identical. But the intensity of the Ni−Ni peak of Ni_3N nanosheets shows a significant decrease. The decreased peak intensity in Ni_3N

DOI: 10.1021/ja5119495
J. Am. Chem. Soc. 2015, 137, 4119−4125

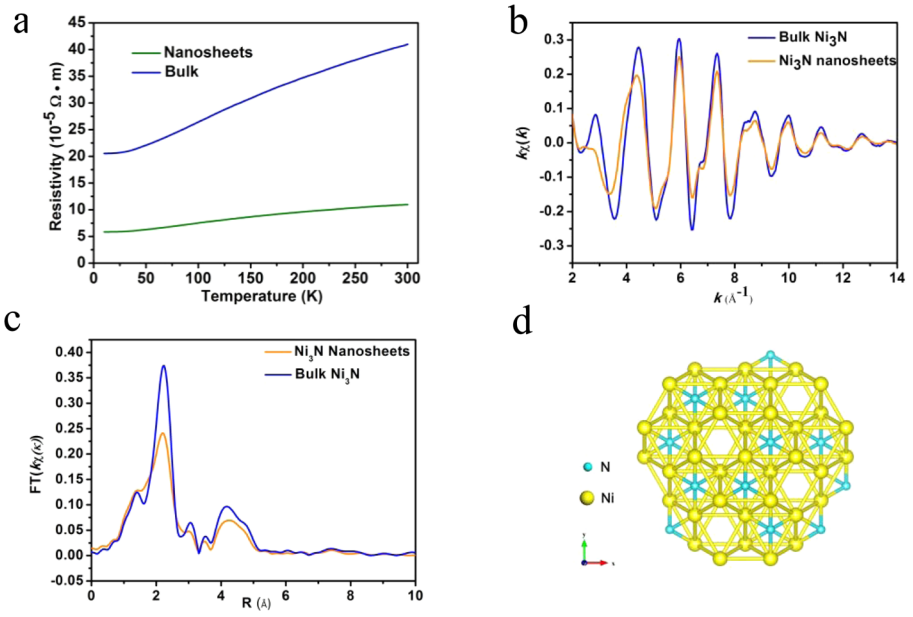

Figure 3. (a) Temperature-dependent electrical resistivity of Ni_3N nanosheet and bulk Ni_3N. (b) Ni K-edge extended EXAFS oscillation and (c) the corresponding Fourier transforms. (d) The sketch of the geometrical structure of Ni_3N crystal viewed from the c-orientation at the range of 6 Å (N atoms: blue; Ni atoms: Yellow).

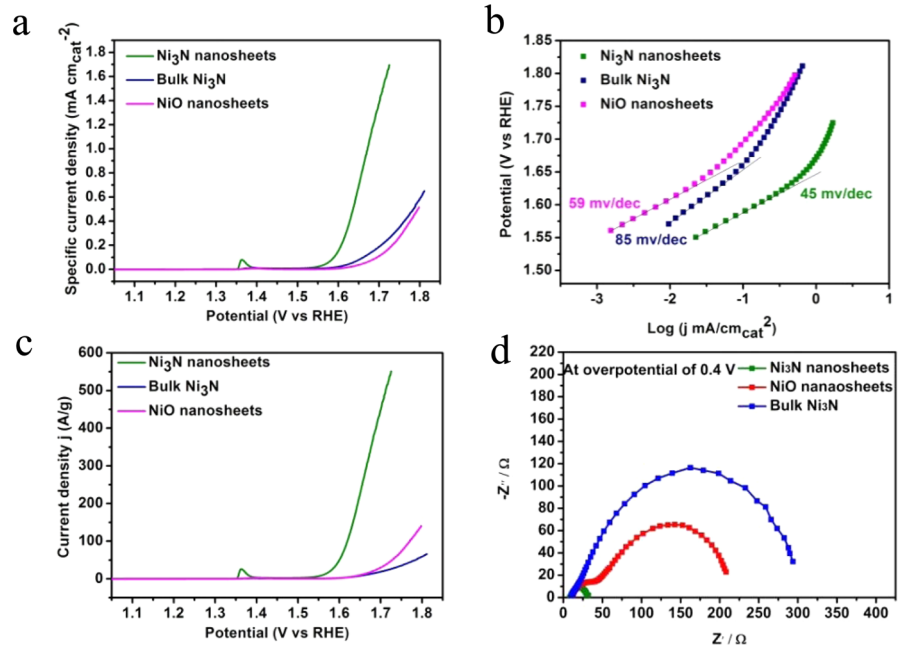

Figure 4. (a) The normalized polarization curves of Ni_3N nanosheets, bulk Ni_3N and NiO nanosheets by the BET surface area of electrocatalysts. (b) Corresponding Tafel plots of Ni_3N nanosheets, bulk Ni_3N and NiO nanosheets. (c) Mass activity of Ni_3N nanosheets, bulk Ni_3N and NiO nanosheets at various applied potentials. (d) Nyquist plots of Ni_3N nanosheets, bulk Ni_3N and NiO nanosheets. Z′ is real impedance and Z″ is imaginary impedance. Note: All the measurements were performed in O_2 saturated 1 M KOH solution.

nanosheets is due to surface structural disorder and Ni coordination missing. In order to obtain quantitative structural information, the Ni−N and Ni−Ni pairs of the EXAFS of both samples were fitted in the real space (R-space), as shown in Figure S16. In the fits, the crystal structure of P6322 space group (Figure 3d) was used to generate the initial structure for EXAFS analysis, according to the XRD characterization. In that model, the absorbed Ni atom is surrounded by 2 N atoms and 12 Ni atoms as the first and second nearest shells, respectively. The fits show the coordination number of the first nearest N shell remains almost 2 and that of the Ni−Ni pair in the nanosheets decreased to 8.7 from 12 for the bulk sample, and the Ni−Ni pair in the nanosheets is a little more disordered than that in the bulk (Table S1). The results give solid evidence that the structure of Ni_3N nanosheets have been disordered with vacancy formation resultant of the dimensional reduction. It is well-known that the disordered structure and vacancy can offer more effective active sites for catalysts.[18,32] On the basis of the above analyses, Ni_3N nanosheets show advantages as a highly efficient electro-

DOI: 10.1021/ja5119495
J. Am. Chem. Soc. 2015, 137, 4119−4125

catalyst for OER arising from following three factors: (1) The intrinsically metallic Ni_3N ensures the contact at the catalyst-electrolyte and catalyst−support electrode interfaces are ohmic contact, unlike Schottky contact, which does not need additional overpotential to overcome it. (2) The faster electron transportation in Ni_3N nanosheets was further enhanced by the dimensional reduction of 2D ultrathin nanostructure. (3) 2D architecture of the electrocatalyst with disordered and defect structure could provide larger surface area, more active sites and realize more intimate contact with the support electrode compared with its bulk counterpart. In this regard, 2D metallic Ni_3N ultrathin nanosheets with enhanced electrochemical performance of electrocatalytic water oxidation are expectable.

To evaluate the OER property of the Ni_3N ultrathin nanosheets, the sample was first deposited onto a glass carbon electrode (GCE), which resulted in a uniform catalyst film with a catalyst loading of 0.285 mg/cm^2. Linear sweep voltammetry (LSV) using the prepared electrode was recorded in O_2-saturated 1 M KOH alkaline solution. Similar tests were also carried out using bulk Ni_3N and NiO nanosheets for comparison. The ohmic potential drop (iR) losses caused by electrolyte resistance, were compensated before comparison. The OER LSV curves using all the samples which have been normalized by the BET surface area of electrocatalyst are shown in Figure 4a. The oxidation peaks located in 1.32 V vs RHE are ascribed to Ni^{II} to Ni^{III}, which have been investigated in detail in most of Ni-based electrocatalysts.[8,12,33] Obviously, the specific current density of Ni_3N nanosheets is indeed higher than that of bulk Ni_3N and NiO nanosheets under a certain applied voltage, also presents a much earlier onset potential, directly confirming that the metallic Ni_3N nanosheets own a higher intrinsic electrocatalytic activity for OER than that of bulk Ni_3N and NiO nanosheets. Moreover, the corresponding Tafel plots (η vs log(j)) were drawn to investigate the OER mechanism using the Ni_3N ultrathin nanosheets (Figure 4b). The Tafel slope using the Ni_3N nanosheets is measured to be 45 mV/dec, which is smaller than using NiO nanosheets (59 mV/dec) and bulk Ni_3N (85 mV/dec). It is noted that, despite a same catalytic structure, the Ni_3N nanosheets have a further decrease in the slope value compared with the bulk Ni_3N. It could be caused by the difference in resistance of materials and of charge transfer on the surface, both of which are found to influence the Tafel slope. As shown in Figure 4c, the OER mass activity of Ni_3N is also much higher than that of NiO nanosheets and bulk Ni_3N. For example, at overpotential of 0.5 V, the mass activity of the Ni_3N nanosheets was 572 A/g, more than 10- and 19-times higher than that of NiO nanosheets (52.5 A/g) and bulk Ni_3N (29.3 A/g). The LSV results, Tafel slope data and OER mass activity results lead to the conclusion that Ni_3N nanosheets are the most efficient electrocatalyst among the materials investigated herein. To further prove better OER electrocatalytic efficiency for Ni_3N nanosheets, EIS was carried out to study the electrode kinetics under OER condition. The Nyquist plots (Figure 4d) unravel that the charge-transfer resistance of the Ni_3N nanosheets exhibited a significantly decrease in comparison with bulk Ni_3N and NiO nanosheets. The finding suggests that Ni_3N nanosheets have the fastest charge transfer process among all three catalysts, which could be associated with the unique electronic structure of 2D Ni_3N and is in good agreement with the outstanding OER property.

Mechanistic studies have proposed that OER on Ni-based catalysts in alkaline electrolyte involves four consequent elementary steps and can be depicted as follows:[34]

$$Ni^{2+} + 3OH^- \leftrightarrow NiOOH + H_2O + e^- \quad (1)$$

$$NiOOH + OH^- \leftrightarrow NiO(OH)_2 + e^- \quad (2)$$

$$NiO(OH)_2 + 2OH^- \leftrightarrow NiOO_2 + 2H_2O + 2e^- \quad (3)$$

$$NiOO_2 + OH^- \rightarrow NiOOH + O_2 + e^- \quad (4)$$

$$\text{Summary OER: } 4OH^- \rightarrow O_2 + 2H_2O + 4e^-$$

Steps 1, 2, and 3 are reversible and determine the overall OER rate, while step 4 is fast and irreversible. The OER on the Ni_3N nanosheets could share a similar mechanism. Surface Ni atoms on the surface are first partially oxidized into NiOOH and form NiOOH/Ni_3N as the actual surface active sites, evidenced by the Ni^{II}-to-Ni^{III} oxidation peak at around 1.4 V vs RHE. The NiOOH/Ni_3N can be further oxidized into $NiOO_2$/Ni_3N at a higher potential, and a further electro-oxidation leads to O_2 evolution and NiOOH/Ni_3N regeneration. The excellent conductivity of metallic Ni_3N nanosheets provides dramatically more efficient electron transportation between electrode and NiOOH/Ni_3N surface active sites compared with insulating NiO nanosheets, which benefits OER on Ni_3N nanosheets with more effective generation of surface active sites and finally much promoted reaction rate. An interesting observation is that the Ni^{II}-to-Ni^{III} oxidation peak for Ni_3N nanosheets is more intense than that for NiO nanosheets despite their similar specific surface areas, implying more active sites formation on the electron conductive Ni_3N.

It needs to be noted that some recently developed Ni-based OER catalysts with excellent property were reported,[35−37] a few of which have even higher OER activity than the metallic Ni_3N nanosheets in this study. These advanced OER catalysts usually have amorphous structure or contain mixed metal elements, demonstrating that factors besides electron conductivity can also influence the OER property. The findings also point to the possibility of further promoting OER on Ni_3N nanosheets by hybridization, doping or further disorder engineering of the catalytic structure. Considering that three-dimensional electrode could bring a larger active surface area in a compact volume and thus achieves a greater geometrical current density favored by practical applications, the metallic Ni_3N nanosheets grown on carbon cloth (CC) electrode has been prepared (S15). As shown in Figure 5a, at overpotential of 0.35 and 0.5 V the geometrical current density for Ni_3N nanosheets/CC was found to be 52.3 and 153.2 mA/cm^2, respectively. To the best of our knowledge, such high current density at low overpotential is among the most efficient OER electrocatalysts (Table S3).[9−16,35−47] In contrast, CC shows a negligible current density at the same overpotential, which further confirms that the high OER activity of our Ni_3N nanosheets. The Ni_3N nanosheets/CC has even smaller Tafel slope and charger transfer resistance compared with Ni_3N nanosheets, which is probably resultant of the complex synergistic effect between Ni_3N nanosheets and CC and accounting for its outstanding OER activity.[47] As is well-known, stability is another key parameter to evaluate electrocatalysts. To assess the stability of the Ni_3N nanosheets for OER in alkaline electrolyte, continuous OER at static overpotential was performed. As shown in Figure 5b, the time dependence of the current density for Ni_3N nanosheeets/CC

DOI: 10.1021/ja5119495
J. Am. Chem. Soc. 2015, 137, 4119−4125

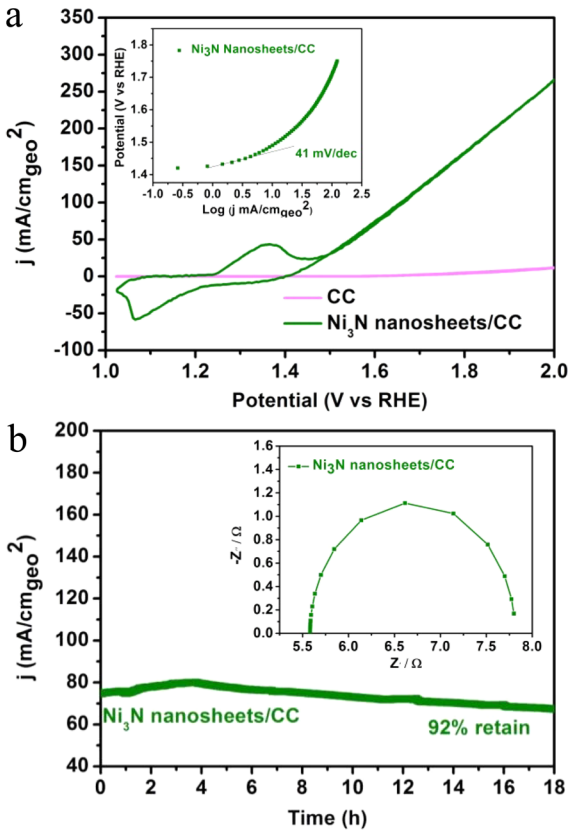

Figure 5. (a) Cyclic voltammetry curves of carbon cloth (CC) and Ni_3N nanosheets/CC. Inset: the Talfe slope of Ni_3N nanosheets/CC. Note: the cathodic sweep was used as OER current for Tafel plots of Ni_3N nanosheets/CC to avoid the interference of oxidation peak in Ni_3N nanosheets/CC. (b) Chronopotentiometry of Ni_3N nanosheets/CC at a overpotential of 0.4 V. Inset: Nyquist plots of Ni_3N nanosheets/CC. Note: All the measurements were performed in O2 saturated 1 M KOH solution.

at an overpotential of 400 mV shows only a little degradation even after a long period of 18 h, suggesting the Ni_3N nanosheets are of excellent stability for electrochemical water oxidation. All above results have demonstrated that the Ni_3N nanosheets possess superior OER activity as well as great durability, endowing it a promising OER electrocatalyst for future applications.

In summary, we have successfully developed a new 2D metallic Ni-based material, Ni_3N nanosheets below 3 nm, as an efficient OER catalyst. Because of the enhanced metallic electrical conductivity behavior and disorder structure, Ni_3N nanosheets exhibit enhanced OER catalytic activity compared with bulk Ni_3N and NiO nanosheets, with earlier onset potential and a smaller Tafel slope of 45 mV/dec. Furthermore, Ni_3N nanosheets grown on carbon cloth could achieve an ultrahigh geometrical current density of 52.3 mA/cm^2 at a relative low overpotential of 350 mV. This work paves a new pathway for designing high efficient OER electrocatalysts based on conducting materials, as well as inspires more scientific interest in 2D metallic materials catering for the field of energy storage and conversion.

■ ASSOCIATED CONTENT

Supporting Information

XRD patterns, SEM images, TEM images, EDX, elemental mapping, BET and additional electrochemical date. This material is available free of charge via the Internet at http://pubs.acs.org.

■ AUTHOR INFORMATION

Corresponding Authors

*czwu@ustc.edu.cn
*chuws@ustc.edu.cn
*zpeng@uakron.edu

Author Contributions

⊥K.X. and P.C. contributed equally.

Notes

The authors declare no competing financial interest.

■ ACKNOWLEDGMENTS

This work was financially supported by the National Basic Research Program of China (2015CB932302), National Natural Science Foundation of China (No. 21222101, U1432133, 11132009, 21331005, 11321503, J1030412), Chinese Academy of Science (XDB01020300), the Fok Ying-Tong Education Foundation, China (Grant No. 141042), and the Fundamental Research Funds for the Central Universities (No. WK2060190027).

■ REFERENCES

(1) Gray, H. B. *Nat. Chem.* **2009**, *1*, 7.
(2) Cook, T. R.; Dogutan, D. K.; Reece, S. Y.; Surendranath, Y.; Teets, T. S.; Nocera, D. G. *Chem. Rev.* **2010**, *110*, 6474.
(3) Cheng, F.; Chen, J. *Chem. Soc. Rev.* **2012**, *41*, 2172.
(4) Zhao, Y.; Nakamura, R.; Kamiya, K.; Nakanishi, S.; Hashimoto, K. *Nat. Commun.* **2013**, *4*, 2390.
(5) Suntivich, J.; May, K. J.; Gasteiger, H. A.; Goodenough, J. B.; Shao-Horn, Y. *Science* **2011**, *334*, 1383.
(6) Lee, Y.; Suntivich, J.; May, K. J.; Perry, E. E.; Shao-Horn, Y. *J. Phys. Chem. Lett.* **2012**, *3*, 399.
(7) Lyons, M. E. G.; Floquet, S. *Phys. Chem. Chem. Phys.* **2011**, *13*, 5314.
(8) Smith, R. D. L.; Prévot, M. S.; Fagan, R. D.; Trudel, S.; Berlinguette, C. P. *J. Am. Chem. Soc.* **2013**, *135*, 11580.
(9) Kuai, L.; Geng, J.; Chen, C.; Kan, E.; Liu, Y.; Wang, Q.; Geng, B. *Angew. Chem., Int. Ed.* **2014**, *53*, 7547.
(10) Fominykh, K.; Feckl, J. M.; Sicklinger, J.; Döblinger, M.; Böcklein, S.; Ziegler, J.; Peter, L.; Rathousky, J.; Scheidt, E.-W.; Bein, T.; Fattakhova-Rohlfing, D. *Adv. Funct. Mater.* **2014**, *24*, 3123.
(11) Gao, M.; Sheng, W.; Zhuang, Z.; Fang, Q.; Gu, S.; Jiang, J.; Yan, Y. *J. Am. Chem. Soc.* **2014**, *136*, 7077.
(12) Trotochaud, L.; Young, S. L.; Ranney, J. K.; Boettcher, S. W. *J. Am. Chem. Soc.* **2014**, *136*, 6744.
(13) Gong, M.; Li, Y.; Wang, H.; Liang, Y.; Wu, J. Z.; Zhou, J.; Wang, J.; Regier, T.; Wei, F.; Dai, H. *J. Am. Chem. Soc.* **2013**, *135*, 8452.
(14) Chen, S.; Duan, J.; Jaroniec, M.; Qiao, S. Z. *Angew. Chem., Int. Ed.* **2013**, *52*, 13567.
(15) Long, X.; Li, J.; Xiao, S.; Yan, K.; Wang, Z.; Chen, H.; Yang, S. *Angew. Chem., Int. Ed.* **2014**, *53*, 7584.
(16) Song, F.; Hu, X. *Nat. Commun.* **2014**, *5*, 4477.
(17) Zhou, W.; Wu, X.-J.; Cao, X.; Huang, X.; Tan, C.; Tian, J.; Liu, H.; Wang, J.; Zhang, H. *Energy Environ. Sci.* **2013**, *6*, 2921.
(18) Xie, J.; Zhang, J.; Li, S.; Grote, F.; Zhang, X.; Zhang, H.; Wang, R.; Lei, Y.; Pan, B.; Xie, Y. *J. Am. Chem. Soc.* **2013**, *135*, 17881.
(19) Matsumoto, Y.; Sato, E. *Mater. Chem. Phys.* **1986**, *14*, 397.
(20) Sun, Y.; Sun, Z.; Gao, S.; Cheng, H.; Liu, Q.; Piao, J.; Yao, T.; Wu, C.; Hu, S.; Wei, S.; Xie, Y. *Nat. Commun.* **2012**, *3*, 1057.
(21) Sun, Y.; Gao, S.; Lei, F.; Xie, Y. *Chem. Soc. Rev.* **2015**, *44*, 623.

DOI: 10.1021/ja5119495
J. Am. Chem. Soc. 2015, 137, 4119−4125

(22) Chen, W.-F.; Sasaki, K.; Ma, C.; Frenkel, A. I.; Marinkovic, N.; Muckerman, J. T.; Zhu, Y.; Adzic, R. R. *Angew. Chem., Int. Ed.* **2012**, *51*, 6131.
(23) Ida, S.; Shiga, D.; Koinuma, M.; Matsumoto, Y. *J. Am. Chem. Soc.* **2008**, *130*, 14038.
(24) Gajbhiye, N. S.; Ningthoujam, R. S.; Weissmüller, J. *Phys. Status Solidi A* **2002**, *189*, 691.
(25) Hohenberg, P.; Kohn, W. *Phys. Rev.* **1964**, *136*, B864.
(26) Kohn, W.; Sham, L. J. *Phys. Rev.* **1965**, *140*, A1133.
(27) Kresse, G.; Furthmüller, J. *Phys. Rev. B: Condens. Matter Mater. Phys.* **1996**, *54*, 11169.
(28) Kresse, G.; Joubert, D. *Phys. Rev. B: Condens. Matter Mater. Phys.* **1999**, *59*, 1758.
(29) Perdew, J. P.; Burke, K.; Ernzerhof, M. *Phys. Rev. Lett.* **1996**, *77*, 3865.
(30) Blöchl, P. E. *Phys. Rev. B: Condens. Matter Mater. Phys.* **1994**, *50*, 17953.
(31) Lu, X.; Wang, G.; Zhai, T.; Yu, M.; Xie, S.; Ling, Y.; Liang, C.; Tong, Y.; Li, Y. *Nano Lett.* **2012**, *12*, 5376.
(32) Kibsgaard, J.; Chen, Z.; Reinecke, B. N.; Jaramillo, T. F. *Nat. Mater.* **2012**, *11*, 963.
(33) Louie, M. W.; Bell, A. T. *J. Am. Chem. Soc.* **2013**, *135*, 12329.
(34) Juodkazis, K.; Juodkazytė, J.; Vilkauskaitė, R.; Jasulaitienė, V. *J. Solid State Electrochem.* **2008**, *12*, 1469.
(35) Trotochaud, L.; Ranney, J. K.; Williams, K. N.; Boettcher, S. W. *J. Am. Chem. Soc.* **2012**, *134*, 17253.
(36) Yang, Y.; Fei, H.; Ruan, G.; Xiang, C.; Tour, J. M. *ACS Nano* **2014**, *8*, 9518.
(37) Smith, R. D. L.; Prévot, M. S.; Fagan, R. D.; Zhang, Z.; Sedach, P. A.; Siu, M. K. J.; Trudel, S.; Berlinguette, C. P. *Science* **2013**, *340*, 60.
(38) Song, F.; Hu, X. *J. Am. Chem. Soc.* **2014**, *136*, 16481.
(39) McCrory, C. C. L.; Jung, S.; Peters, J. C.; Jaramillo, T. F. *J. Am. Chem. Soc.* **2013**, *135*, 16977.
(40) Mao, S.; Wen, Z.; Huang, T.; Hou, Y.; Chen, J. *Energy Environ. Sci.* **2014**, *7*, 609.
(41) Kim, J.; Yin, X.; Tsao, K.-C.; Fang, S.; Yang, H. *J. Am. Chem. Soc.* **2014**, *136*, 14646.
(42) Gao, M.-R.; Cao, X.; Gao, Q.; Xu, Y.-F.; Zheng, Y.-R.; Jiang, J.; Yu, S.-H. *ACS Nano* **2014**, *8*, 3970.
(43) Liu, Y.; Cheng, H.; Lyu, M.; Fan, S.; Liu, Q.; Zhang, W.; Zhi, Y.; Wang, C.; Xiao, C.; Wei, S.; Ye, B.; Xie, Y. *J. Am. Chem. Soc.* **2014**, *136*, 15670.
(44) Liu, X.; Chang, Z.; Luo, L.; Xu, T.; Lei, X.; Liu, J.; Sun, X. *Chem. Mater.* **2014**, *26*, 1889.
(45) Zhao, A.; Masa, J.; Xia, W.; Maljusch, A.; Willinger, M.-G.; Clavel, G.; Xie, K.; Schlögl, R.; Schuhmann, W.; Muhler, M. *J. Am. Chem. Soc.* **2014**, *136*, 7551.
(46) Tüysüz, H.; Hwang, Y.; Khan, S.; Asiri, A.; Yang, P. *Nano Res.* **2013**, *6*, 47.
(47) Ma, T. Y.; Dai, S.; Jaroniec, M.; Qiao, S. Z. *J. Am. Chem. Soc.* **2014**, *136*, 13925.

DOI: 10.1021/ja5119495
J. Am. Chem. Soc. 2015, 137, 4119−4125